



Gambling demon and stopping-time fluctuation relation of a Brownian particle under a time-dependent trapping potential

John A. C. Albay,^{1,2} Yonggun Jun (전용근) ^{1,*} and Pik-Yin Lai (黎璧賢) ^{1,3,†}

¹*Department of Physics and Center for Complex Systems, National Central University, Chung-Li District, Taoyuan City 320, Taiwan, Republic of China*

²*Department of Mathematics and Physics, College of Science, University of Santo Tomas, Manila 1015, Philippines*

³*Physics Division, National Center for Theoretical Sciences, Taipei 10617, Taiwan, Republic of China*



(Received 6 October 2023; accepted 30 November 2023; published 19 January 2024)

A gambling demon is an external agent that can terminate a time-dependent driving protocol when a certain observable of the system exceeds a prescribed threshold. The gambling demon is examined in detail both theoretically and experimentally in a Brownian particle system under a compressing potential trap. Insight for choosing an appropriate work threshold for stopping is discussed. The energetics and the distributions of the stopping positions and stopping times are measured in simulations to gain further understanding of the process. Furthermore, the nonstationary and far-from-equilibrium stochastic process in the action of the gambling demon allows us to examine in detail some fundamental issues in stochastic thermodynamics, such as irreversibility and stopping-time fluctuation relation. Paradoxical violation of the stopping-time fluctuation relation can be reconciled in terms of the entropy production associated with fast hidden internal degrees of freedom. All the simulation or theoretical results are confirmed experimentally.

DOI: [10.1103/PhysRevE.109.014124](https://doi.org/10.1103/PhysRevE.109.014124)

I. INTRODUCTION

The breakthrough in nonequilibrium statistical mechanics and fluctuation relations [1–4] in the last few decades allowed a quantitative description for stochastic nonstationary processes in the mesoscopic scale that is far from equilibrium. Remarkably, it is now well-demonstrated that it is possible to have Second Law violating rare events on the trajectory level. With the advances in stochastic thermodynamics [5] and experimental techniques [6–8], one can manipulate and even control these far-from-equilibrium processes [9–11] in strongly fluctuating environment and quantitatively predict their properties [12–15], even under sophisticated feedback protocols.

Frontier topics, such as the thermodynamic theory in mesoscopic systems for stochastic trajectories that terminate at some stopping times once some criterion is reached, which is a generalization of the first-passage times, have recently been addressed [16–19]. For steady-state nonequilibrium systems, the stochastic entropy production at stochastic stopping times obeys an integral fluctuation relation [16], and there are universal bounds for the finite-time survival probability of the stochastic work extraction and heat dissipation [17]. On the other hand, for the more challenging case of nonstationary processes, there is also a thermodynamic bound [19] for the work exerted by an external time-dependent protocol averaged over all trajectories with stochastic stopping times, which can be viewed as a generalization of the usual Second Law of thermodynamics. Furthermore, an integral fluctuation

relation, termed stopping-time integral fluctuation theorem, was derived [18], which constrains the dissipative work in these nonstationary processes with stopping criterion.

Exploiting the information on the stochastic work extraction by stopping the process at an appropriate chosen moment is the working principle of the “gambling demon” that can extract useful work in far-from-equilibrium nonstationary protocols [20]. Recently, we realized experimentally a gambling demon to extract work with a prescribed stopping threshold of cumulative work in the paradigm system of a Brownian particle in a time-dependent squeezing potential trap [21]. The mechanism for the demon to win over the Second Law of Thermodynamics (i.e., having a negative dissipative work) is analyzed by sorting out the statistics of the stopped trajectories, which further leads to improved strategies of time-dependent stopping threshold to enhance the winning profits.

The nonstationary stochastic process of the gambling demon under a compressing trap also allows us to examine in detail some fundamental issues in stochastic thermodynamics. By considering the time-reversed process, the gambling demon provides a convenient platform to investigate the irreversibility and stopping-time fluctuation theorem. In this paper, we investigate the action of the gambling demon under a squeezing potential trap theoretically by Langevin dynamics simulations and also experimentally. The energetics, stopping positions, stopping times, and their distributions are investigated in detail. The time-reversed protocol of the gambling demon is considered to examine the irreversibility and entropy production in the demon’s action. The stopping-time integral fluctuation relation is tested and its apparent deviation can be understood in terms of the hidden internal degrees of freedom that cannot be observed directly under the mesoscopic

*yonggun@phy.ncu.edu.tw

†pylai@phy.ncu.edu.tw

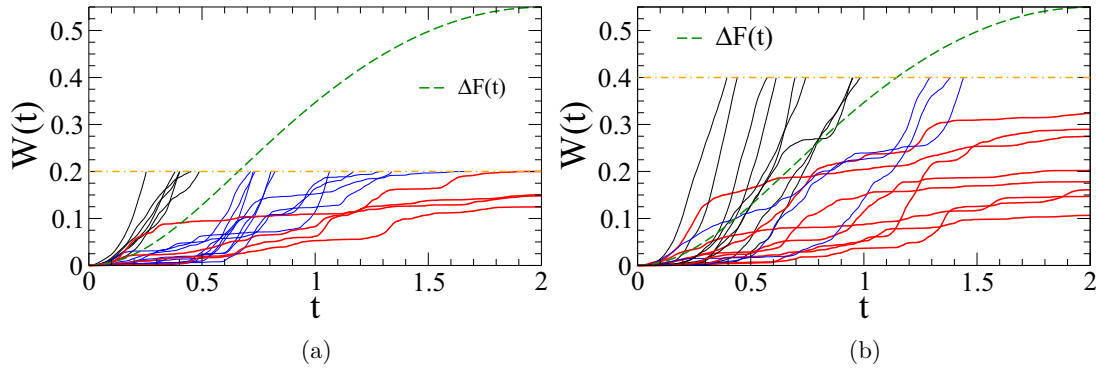


FIG. 1. Simulation results of the work evolution trajectories of the gambling demon under the harmonic potential $U(x, \lambda(t)) = \frac{1}{2}\lambda(t)x^2$ with compressing protocol $\frac{\lambda(t)}{\lambda(0)} = 2 - \cos \frac{\pi t}{\tau}$ with $\tau = 2$. Twenty trajectories are shown in each graph. The threshold W_{th} is marked by the horizontal dot-dashed line. The instantaneous free energy change, $\Delta F(t) = \frac{1}{2} \ln \frac{\lambda(t)}{\lambda(0)}$, is denoted by the dashed curve. (a) $W_{\text{th}} = 0.2$. (b) $W_{\text{th}} = 0.4$.

framework in stochastic thermodynamics. Furthermore, our study is related to stopping processes or generalized first-passage time problems in nonsteady nonequilibrium systems and is also relevant in the use of Martingale theory in stochastic thermodynamics [22].

II. THE GAMBLING DEMON AND THE ASSOCIATED ENERGETICS

The nonstationary external driving is denoted by some arbitrary protocol $\lambda(t)$ that changes one state to another in the time interval $0 \leq t \leq \tau$. The stochastic system is allowed to evolve from some initial state, which can be taken to be at equilibrium, under the action of the potential $U(x, \lambda(t))$ to some final state. The nonsteady process is, in general, far from equilibrium that abides by the traditional Second Law of thermodynamics [23] which guarantees that the mean work done on the system cannot be less than the free energy change, *i.e.*, $\langle W \rangle \geq \Delta F$, when averaged over many trajectories. The difference in the mean work and the free energy change, $\langle W_{\text{diss}} \rangle = \langle W \rangle - \Delta F$, is the mean dissipative work for the process. One can view the nonequilibrium Second Law abiding or violating trajectories, respectively, as winning or losing in a gambling process in which a negative (positive) dissipative work W_{diss} is regarded as a winning (losing) scenario. Then with the decision to stop the process when the cumulative work (betting capital) exceeds some assigned threshold (denoted by W_{th}), the stochastic stopping process of a nonequilibrium trajectory is viewed as the action of a gambling demon, which has been recently realized in an electron box experiment [20] and a Brownian particle under a squeezing harmonic potential [21]. As revealed in

Ref. [21] the key idea for the gambling demon to achieve winning is to exploit the stopping action for two major goals. The first is to cut the expected and potentially big losses by early stopping when the cumulative work reaches the threshold. The second is to stop and harvest some appropriate winning profit without taking the risk until the end of the journey. Figure 1 shows the work trajectories under the action of a gambling demon with a given W_{th} . Only a small fraction of the trajectories can complete their journey (red trajectories) for a low value of W_{th} as shown in Fig. 1(a). Throughout

this paper, the energetic quantities such as work, heat, or free energy are in units of $k_B T$, where k_B is the Boltzmann constant and T is the temperature. Time t is in units of the characteristic relaxation time τ_R which is given by the ratio of the drag coefficient of the Brownian particle to the initial spring constant of the harmonic trap. The number of trajectories without being interrupted by the demon (red trajectories) increases with W_{th} [see Fig. 1(b)]. These noninterrupted trajectories are always winning with $W_{\text{diss}} < 0$. On the other hand, those trajectories that are stopped by the demon can be winning (blue trajectories) or losing (black trajectories). Those losing and stopped trajectories (black trajectories) are essential for the demon to achieve winning on average by cutting big losses in the early stopped events. Those winning and stopped trajectories (blue trajectories) reflect the active role of the demon to gain winning profits. The uninterrupted winning trajectories (red trajectories) in which the demon takes no action, are not the dominant factor in achieving winning. The detailed statistics of these three types of trajectories have been analyzed in Ref. [21]. For each trajectory, the instantaneous work $W(t)$ is monitored, and a binary information of $W(t)$ is less than W_{th} or not is used for the stopping decision. While the acquisition of 1-bit memory does not require energy, resetting 1-bit of memory to acquire another new information costs $k_B T \ln 2$, as given by Landauer's principle [8,24]. Here, we implicitly assume the gambling demon has a very large memory capacity and it does not need to erase information during its action.

Under the action of the gambling demon, the ensemble average of an observable O is $\langle O \rangle_{t_s} \equiv \sum_{x[0, t_s]} P(x[0, t_s]) O(t_s, x[0, t_s])$ with stochastic stopping times t_s , where $x[0, t_s]$ denotes a trajectory that ends at some t_s whose probability is $P(x[0, t_s])$. For an explicit squeezing trap protocol, we consider the potential trap of the form

$$U(x, \lambda(t)) = \frac{1}{2} \lambda(t) x^n, \quad n = 2, 4, \dots \quad (1)$$

$$\text{with } \lambda(t) = \lambda(0) \left[1 + b \left(1 - \cos \frac{\pi t}{\tau} \right) \right], \quad (2)$$

where $b > 0$ and τ is the driving duration. In most cases, we take $b = 1$ and λ has a threefold increase when the squeezing process is completed. The corresponding instantaneous free

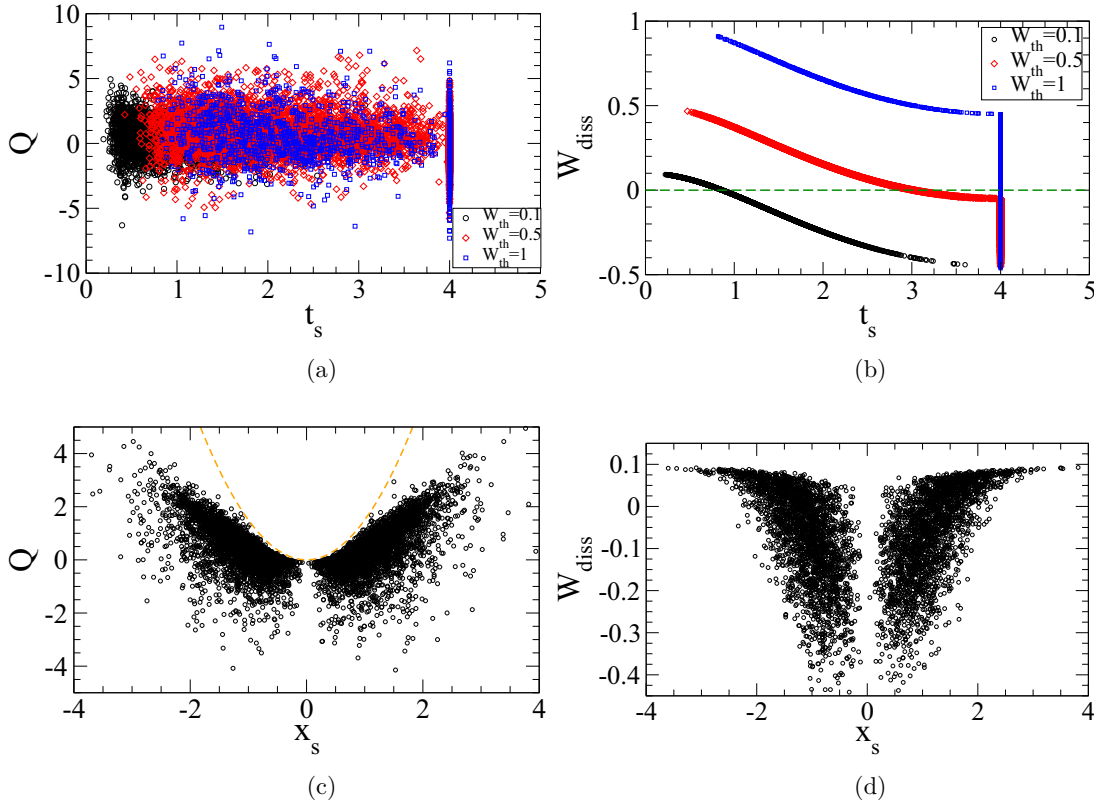


FIG. 2. Energetic quantities of the gambling demon trajectories under the compressing harmonic protocol for the potential $U(x, \lambda(t)) = \frac{1}{2}\lambda(t)x^2$ with $\frac{\lambda(t)}{\lambda(0)} = 2 - \cos \frac{\pi t}{\tau}$ with $\tau = 4$. 8000 trajectories are used. (a) Heat Q , (b) dissipative work W_{diss} vs t_s for various values of W_{th} . (c) Q plotted against the stopped position x_s for $W_{\text{th}} = 0.1$. The trapping potential at $t = \tau$ is shown by the dashed curve. (d) W_{diss} plotted against the stopped position x_s for $W_{\text{th}} = 0.1$.

energy change can be calculated to give $\Delta F(t) = \frac{1}{n} \ln \frac{\lambda(t)}{\lambda(0)}$. In most cases, we focus on the paradigm case of a Brownian particle under a harmonic potential with $n = 2$. An anharmonic trap with $n = 4$ is also considered in some simulation studies. We first carry out simulations by generating stochastic trajectories from the solution of the overdamped Langevin equation $\dot{x}(t) = -\frac{n}{2\gamma}\lambda(t)x^{n-1} + \xi(t)$, where γ is the drag coefficient and ξ is a zero-mean white noise with $\langle \xi(t)\xi(t') \rangle = \frac{2k_B T}{\gamma} \delta(t - t')$. The Langevin equation is solved numerically using the Euler-Maruyama scheme with a time step of $\delta t = 2 \times 10^{-4}$, where time is in the unit of the characteristic relaxation time $\tau_R = \frac{\gamma}{k_B T} (\frac{k_B T}{\lambda(0)})^{2/n}$ and all distances are in units of $(\frac{k_B T}{\lambda(0)})^{1/n}$. Ensemble averages are computed using 5000 to 20 000 stochastic trajectories under the action of the demon.

Figures 2(a) and 2(b) show the Langevin dynamic simulations results of the stochastic heat and dissipative work as a function of the stopped time t_s , of the Brownian system under various stopping thresholds of the gambling demon. The stochastic heat has large fluctuations, and the trajectories are stopped at a later time for larger W_{th} . On the other hand, the stochastic W_{diss} has a smooth dependence on the stopped time which can be understood from the action of the demon to stop the trajectory at $W = W_{\text{th}}$, hence $W_{\text{diss}}(t_s) = W_{\text{th}} - \Delta F(t_s)$ for $t_s < \tau$. On the other hand, for unstopped trajectories with $t_s = \tau$, $W_{\text{diss}}(\tau) = W(\tau) - \Delta F(\tau)$, which is stochastic but its value is $\leq W_{\text{th}} - \Delta F(\tau)$. More information can be revealed by examining the energetics as a function of the stopped

position x_s . Figure 2(c) shows the general trend of more heat flow to the system for trajectories stopped far away from the potential well center, and heat can be extracted from the system if it is stopped closer to the well center. Figure 2(c) indicates that the heat is bound by $\frac{1}{2}\lambda(\tau)x_s^2$ (the dashed curve) which follows from the First Law of thermodynamics $Q = \Delta U - W$ with $W > 0$ for compression, which gives $Q < \Delta U = \frac{1}{2}\lambda(t_s)x_s^2 - \frac{1}{2}\lambda(0)x(0)^2 \simeq \frac{1}{2}\lambda(t_s)x_s^2 \leq \frac{1}{2}\lambda(\tau)x_s^2$. Fig. 2(d) shows that trajectories stopped very far away from the well center are always losing and the majority winning profit trajectories (W_{diss} negative) are stopped at locations within a distance of $\sim \sqrt{\frac{k_B T}{\lambda(0)}}$ inside the well.

The distribution functions of various energetic quantities are displayed in Fig. 3. The work W is always positive due to the compressing potential. $P(W)$ displays an abrupt truncation due to the stopping action of the demon for smaller values of W_{th} [see Fig. 3(a)]. The associated jump at $W = W_{\text{th}}$ is due to the large number of stopped trajectories for small W_{th} , but no such abrupt jump occurs for large W_{th} since nearly all trajectories completed their trips. The stochastic heat for the trajectories shows broad distribution [see Fig. 3(b)], indicating the strong fluctuating nature of heat exchange with the environment. The stopping times and locations of the particles can reveal the situation when the particle is stopped by the demon. The x_s vs t_s scattered plot of the stopped particle shown in Fig. 3(c) reveals that the particles stopped near the well center can complete their journeys, and there

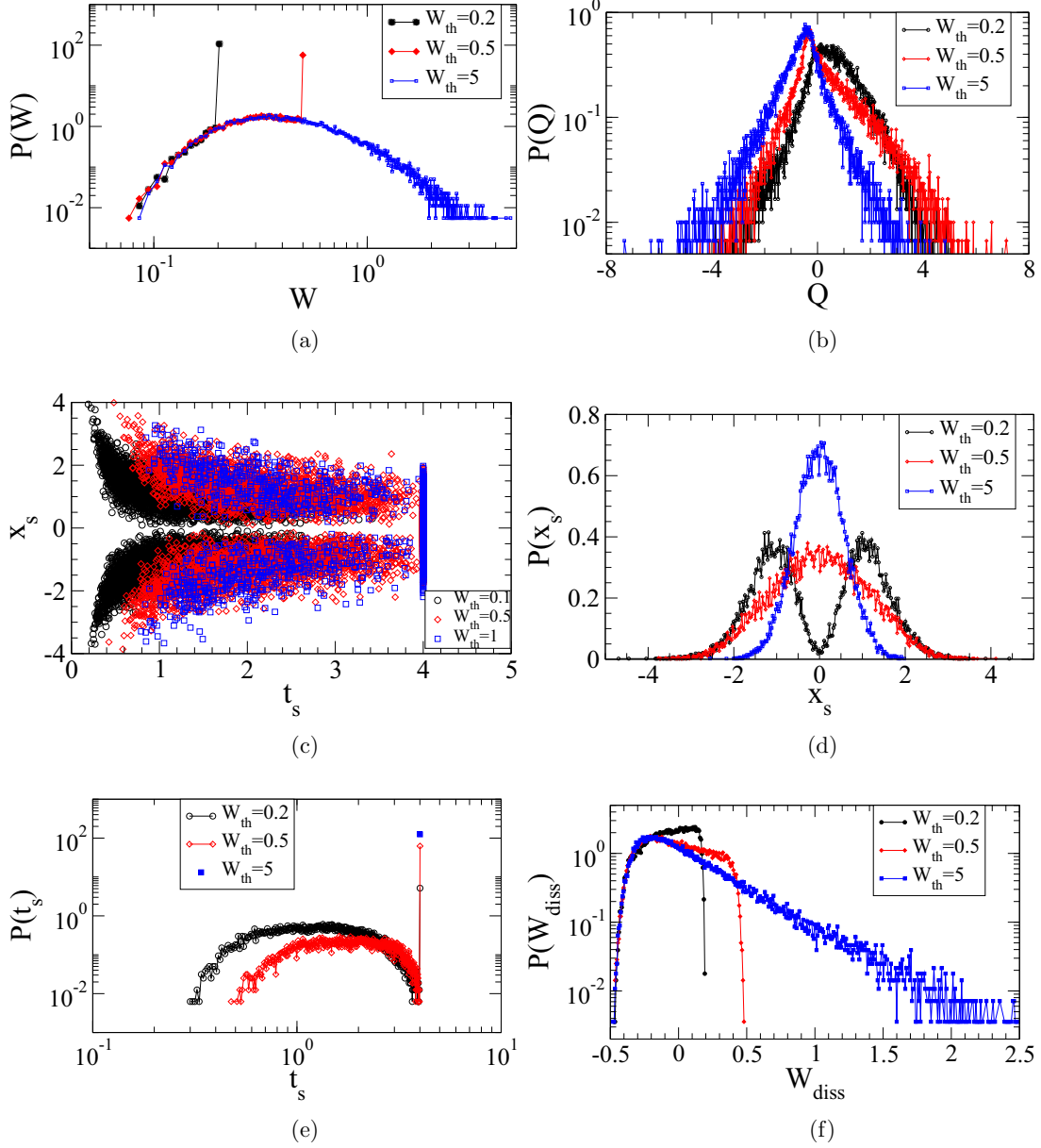


FIG. 3. Simulation results for the harmonic potential $U(x, \lambda(t)) = \frac{1}{2}\lambda(t)x^2$ with compressing protocol $\frac{\lambda(t)}{\lambda(0)} = 2 - \cos \frac{\pi t}{\tau}$ with $\tau = 4$. (a) Work distribution $P(W)$. (b) Heat distribution $P(Q)$. (c) The stopped position x_s plotted against the stopped time t_s with $\tau = 4$ for various values of W_{th} . (d) Stopped distance distribution $P(x_s)$. (e) Stopped time distribution $P(t_s)$. (f) Distribution of the dissipative work W_{diss} .

is a tendency that particles stopped early are further away from the well center. The distribution of the stopped position [see Fig. 3(d)], x_s , changes from the unimodal peak at the well center for large W_{th} (where most trajectories complete their trips) and gets broadened as W_{th} decreases. And for the tight threshold of small W_{th} , the distribution becomes bimodal with a more significant amount of trajectories stopped by the demon, and most particles are stopped significantly away from the well center and very few particles are stopped near the center. For large W_{th} , the stopping time distribution approaches a δ function at $t_s = \tau$ as no trajectory is stopped by the demon [see Fig. 3(e)]. As the work threshold gets small, $P(t_s)$ displays a spectrum of stochastic stopping times due to the action of the demon, superposed with an abrupt peak at $t_s = \tau$ due to the large portion of unstopped trajectories.

The completion peak at $t_s = \tau$ becomes lower for smaller W_{th} as the fraction of unstopped trajectories becomes higher. A winning trajectory is characterized by $W(t_s) < \Delta F(t_s)$, i.e., $W_{diss} < 0$. The stochastic dissipative work distribution under the action of the demon is shown in Fig. 3 f for different values of W_{th} . For large W_{th} , there is no stopping action of the demon and the system obeys the usual fluctuation theorem (W_{diss} is the stochastic total entropy production) and hence an average losing scenario of $\langle W_{diss} \rangle > 0$ is guaranteed. On the other hand, the change of behavior of $P(W_{diss})$ for smaller W_{th} is due to the truncation of large and positive W_{diss} mainly contributed from the losing and stopped trajectories [black trajectories in Fig. 1(a)]. the demo can achieve significant winning for small W_{th} , mainly due to the truncation of large positive (big loss) W_{diss} and an increase in the winning tra-

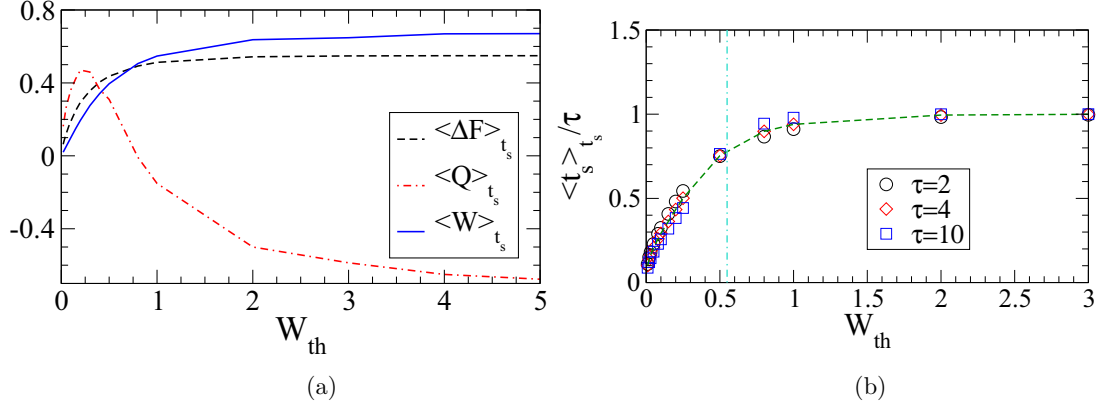


FIG. 4. Simulation results for the harmonic potential $U(x, \lambda(t)) = \frac{1}{2}\lambda(t)x^2$ with compressing protocol $\frac{\lambda(t)}{\lambda(0)} = 2 - \cos \frac{\pi t}{\tau}$. (a) The averaged free energy change, heat and work as a function of the stopping threshold, W_{th} . $\tau = 2$. (b) Normalized mean stopping time $\langle t_s \rangle_{t_s} / \tau$ plotted as a function of W_{th} for various values of τ .

jectories. The mean energetic quantities, $\langle \Delta F \rangle_{t_s}$, $\langle Q \rangle_{t_s}$ and $\langle W \rangle_{t_s}$, averaged over a large number of trajectories under the action of the demon are displayed in Fig. 4(a). $\langle \Delta F \rangle_{t_s}$ increases monotonically with W_{th} and saturates to the value of $\Delta F(\tau)$ ($= \frac{1}{2} \ln 3 \simeq 0.5493$ here) for large values of W_{th} in which all trajectories can complete their trips without being stopped. $\langle W \rangle_{t_s}$ is positive due to the squeezing protocol and is monotonically increasing with saturation towards a value that is greater than $\Delta F(\tau)$. On the other hand, the average heat $\langle Q \rangle_{t_s}$ shows a nonmonotonic behavior with positive mean heat flow into the system for small W_{th} and mean heat flow out of the system as W_{th} becomes large. The dependence of the action of the demon on the threshold can be revealed by plotting the (scaled) average stopping time as a function of W_{th} as displayed in Fig. 4(b). $\langle t_s \rangle_{t_s}$ increases monotonically with W_{th} as expected, and saturation begins to set in for $W_{th} \simeq \Delta F(\tau)$ (denoted by the vertical dashed line). This again indicates that for the demon to be effective, one should choose a threshold that is smaller than $\Delta F(\tau)$ so that a significant number of trajectories are stopped.

The performance of the demon is evaluated by the dissipative work averaged over many trajectories which are plotted as a function of the threshold for different τ 's in Fig. 5(a). $\langle W_{diss} \rangle_{t_s}$ is positive for large values of threshold respecting the usual second law of thermodynamics. But for small values of

W_{th} , $\langle W_{diss} \rangle_{t_s}$ is negative, indicating that useful work can be extracted by the action of the demon. In addition, maximal work can be extracted ($\langle W_{diss} \rangle_{t_s}$ is most negative) for some (small) value of W_{th} . Such a most negative $\langle W_{diss} \rangle_{t_s}$ depends on τ whose dependence is displayed in Fig. 5(b), showing a broad peak around a small value of $\tau \sim 0.08$.

III. CHOOSING THE THRESHOLD W_{th}

As demonstrated by the simulation results in the previous section, one needs to choose W_{th} a couple of times smaller than $\Delta F(\tau)$ for the demon to be effective [see Fig. 4(b)] and to achieve good winning profit [see Fig. 5(a)]. However, with a chosen W_{th} that is too low, we discard some trajectories that could have won more if they were kept for a longer time. A trajectory stopped at $t_s < \tau$ is winning if $t_s > \alpha\tau$, where $0 < \alpha = \alpha(W_{th}) \leq 1$, which can be solved from $\Delta F(\alpha\tau) = W_{th}$. Here, we take advantage of knowing the time dependence of the compressing protocol $\lambda(t)$, and hence the variation of $\Delta F(t)$ is also known precisely. Notice that the stopped trajectory is winning because $\Delta F(t)$ increases faster than the cumulative work, but $\frac{d\Delta F}{dt}$ will slow down once $t > t^*$ where the peak of $\frac{d\Delta F}{dt}$ occurs at t^* [see Fig. 6(a)]. For the potential and compressing protocol in Eqs. (1) and (2), $\alpha(W_{th})$ and t^*

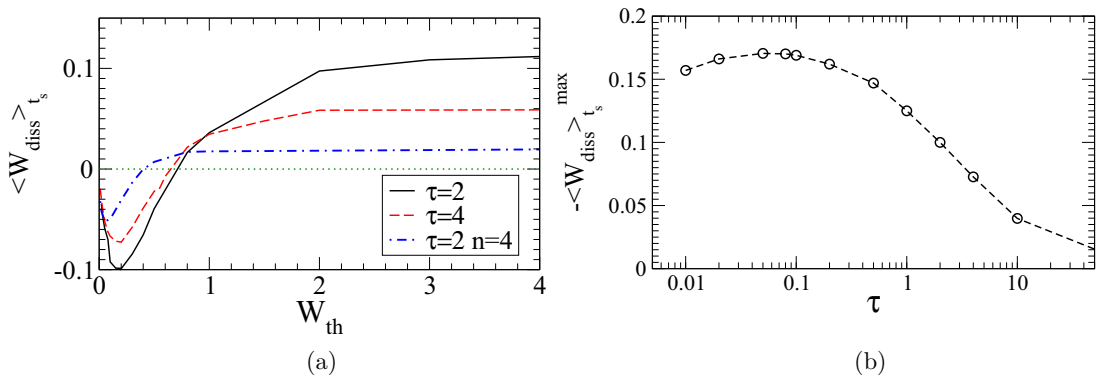


FIG. 5. Simulation results for the harmonic potential $U(x, \lambda(t)) = \frac{1}{2}\lambda(t)x^2$ with compressing protocol $\frac{\lambda(t)}{\lambda(0)} = 2 - \cos \frac{\pi t}{\tau}$. (a) $\langle W_{diss} \rangle_{t_s}$ as a function of W_{th} for $\tau = 2, 4$. The case of anharmonic trap of $\frac{1}{2}\lambda(t)x^4$ for $\tau = 2$ is also shown. (b) Maximal dissipative work (magnitude) measure from the simulation results of the gambling demon vs τ .

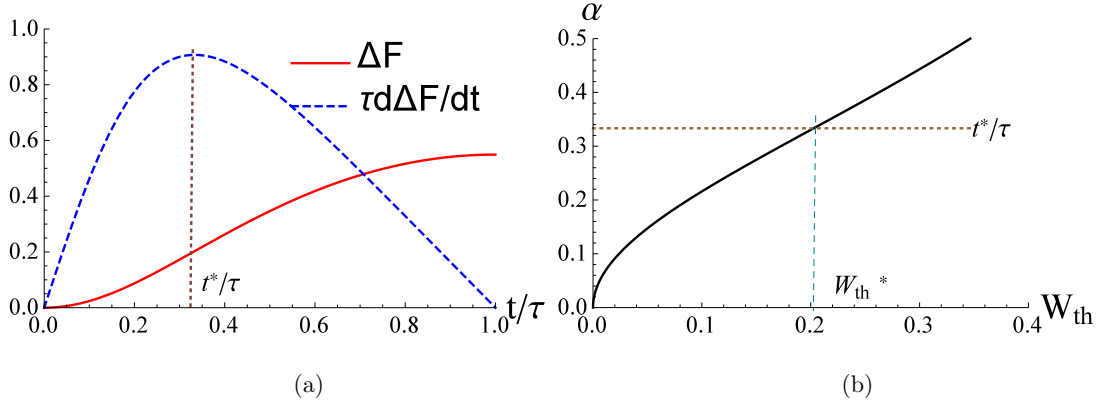


FIG. 6. For harmonic potential $U(x, \lambda(t)) = \frac{1}{2}\lambda(t)x^2$ with compressing protocol $\frac{\lambda(t)}{\lambda(0)} = 2 - \cos \frac{\pi t}{\tau}$. (a) $\Delta F(t)$ and $\tau \frac{d\Delta F}{dt}$ vs $\frac{t}{\tau}$. (b) $\alpha(W_{\text{th}})$ plotted as a function of W_{th} . The horizontal dashed line marks the value of $\alpha = \frac{t^*}{\tau}$.

can be easily obtained to be

$$\alpha(W_{\text{th}}) = \frac{1}{\pi} \cos^{-1} \left(1 + \frac{1}{b} - e^{nW_{\text{th}}} \right), \quad (3)$$

$$\frac{t^*}{\tau} = \frac{1}{\pi} \cos^{-1} \left(\frac{b}{1+b} \right). \quad (4)$$

Figure 6(b) shows the variation of $\alpha(W_{\text{th}})$ for the $n = 2$ harmonic potential. A good choice of W_{th} will allow a winning trajectory to be stopped at t_s with $t^* > t_s > \alpha(W_{\text{th}})\tau$ before $\frac{d\Delta F}{dt}$ slows down. Hence, one should choose $W_{\text{th}} < W_{\text{th}}^*$ where $\alpha(W_{\text{th}}^*)\tau = t^*$ as depicted in Fig. 6(b). In this case W_{th}^* can be solved to give

$$W_{\text{th}}^* = \frac{1}{n} \ln \frac{1+2b}{b(1+b)}. \quad (5)$$

For $b = 1$, one gets $W_{\text{th}}^* = 0.202$ for the harmonic trap. As shown in the simulation results in Fig. 5(a), optimal winning is achieved ($\langle W_{\text{diss}} \rangle$ most negative) around $W_{\text{th}} < W_{\text{th}}^*$. Similarly, $W_{\text{th}}^* = 0.101$ for the case of nonharmonic trap with $\frac{1}{2}\lambda(t)x^4$, and a high winning is confirmed from the simulation results in Fig. 5(a). For general protocol of the form $\lambda(t) = \Lambda(\frac{t}{\tau})$ and general trapping potential of the form given by Eq. (1), W_{th}^* can be obtained by first finding the root α^* from $\Lambda(\alpha^*)\dot{\Lambda}(\alpha^*) = \dot{\Lambda}^2(\alpha^*)$, and a suitable choice of the threshold is then given by $W_{\text{th}} \lesssim W_{\text{th}}^* = \frac{1}{n} \ln \frac{\Lambda(\alpha^*)}{\Lambda(0)}$.

IV. IRREVERSIBILITY AND STOPPING-TIME FLUCTUATION RELATION

We first examine the irreversibility of the nonstationary driving process of $\lambda(t)$ without the action of the demon. One considers the reverse protocol that starts to drive the system immediately after the end of the forward protocol with $\lambda_R(t) = \lambda(\tau - t)$ for the same duration τ . The irreversibility for a trajectory at a time $0 \leq t \leq \tau$ is given by the log-ratio of the probabilities of the particle in the forward process at time t to that of the reverse one when it is played back for the same duration:

$$\delta(t) = \ln \frac{P(x(t), t)}{P_R(x(t), \tau - t)}, \quad (6)$$

where $P(x, t)$ and $P_R(x, t)$ are the position probability distribution functions in the forward and reverse processes,

respectively. The process is irreversible if $P(x, t)$ and $P_R(x, \tau - t)$ are distinct. Figure 7(a) shows the simulation results of the forward and reverse distributions at some given time which clearly indicate the irreversible nature of the nonstationary protocol. It is easy to see from the definition of $\delta(t)$ in Eq. (6) that it obeys the integral fluctuation relation:

$$\begin{aligned} \langle e^{-\delta(t)} \rangle &= \int dx P(x, t) \frac{P_R(x, \tau - t)}{P(x, t)} \\ &= 1, \text{ for } 0 \leq t \leq \tau, \end{aligned} \quad (7)$$

which in turn gives

$$\langle \delta(t) \rangle \geq 0, \quad (8)$$

exemplifying the irreversibility nature or ‘‘Second Law’’ for general nonequilibrium processes. Notice that $\delta(\tau) = 0$ since the initial configuration of the reverse process is, by definition, the ending configuration of the forward process, i.e., the system is played back immediately when the forward protocol ends. On the other hand, $\delta(0) \geq 0$ with the equality holds only in the quasistatic limit of an infinitely slow protocol, otherwise, $\delta(0) > 0$ for general finite duration protocols in nonequilibrium processes.

The ensemble average of the stochastic distinguishability of the forward and reverse trajectories up to time t defined in Eq. (6) is given by

$$\langle \delta(t) \rangle = \int dx P(x, t) \ln \frac{P(x, t)}{P_R(x, \tau - t)} \equiv \Delta_{KL}(t), \quad (9)$$

which is simply the Kullback-Leibler (KL) divergence of the forward from its reverse distribution that can serve as an alternative measure for the irreversibility at a given time. The irreversibility can also be conveniently characterized by the difference in the variances of $P(x, t)$ and $P_R(x, \tau - t)$. For harmonic potentials, these variances (denoted respectively by $w(t)$ and $w_R(\tau - t)$) can be calculated explicitly and are given by Eq. (A9) and (A11) in the Appendix. The theoretical time-dependent variances of the forward and reverse distributions together with their ratio are plotted in Fig. 7(b), indicating that forward and reverse variances are distinct. In addition, their ratio is a measure of the degree of irreversibility, which is also time-dependent but is always ≥ 1 . The measured variance ratio obtained from simulations is

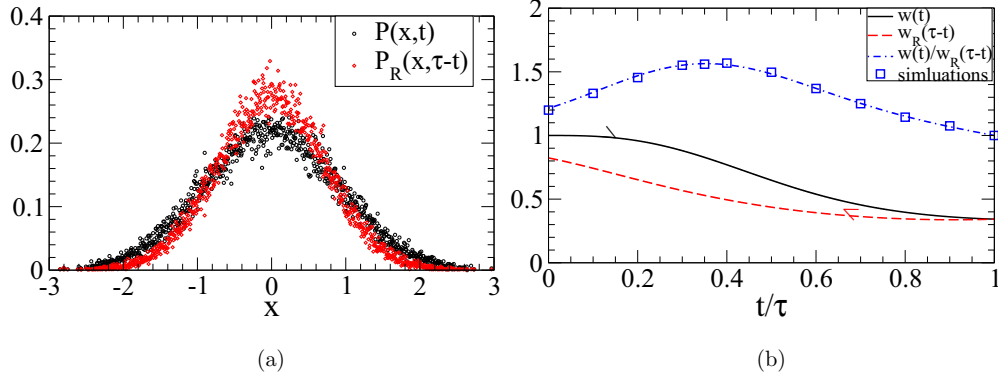


FIG. 7. Brownian particle under the harmonic potential $U(x, \lambda(t)) = \frac{1}{2}\lambda(t)x^2$ with compressing protocol $\frac{\lambda(t)}{\lambda(0)} = 2 - \cos \frac{\pi t}{\tau}$. (a) Simulation results for the forward and reversed position probability distributions at $t = 0.7$ for $\tau = 2$. (b) Theoretical results of $w(t)$ and $w_R(\tau - t)$ and their ratio for $\tau = 2$. Simulation results (\square) are also shown.

also plotted, showing perfect agreement with the theoretical values.

The stochastic distinguishability or irreversibility associated with the action of the gambling demon can be examined by δ at the stopped moment and position, which are shown in the scattered plots in Fig. 8(a) and 8(b). Here, $\delta(t)$ is obtained using Eq. (6) by measuring the forward and reverse position distributions. There is a general trend of stronger irreversibility when the particle is stopped at earlier times and stopped at positions further away from the trap center. The degree of irreversibility can be quantitatively revealed by $\delta(t)$ averaged over the stopped trajectories. Figure 9(a) shows the simulation results of $\langle \delta \rangle_{t_s}$ that peaks for some

characteristic W_{th} at which the process is most irreversible. This can be understood from the KL-divergence irreversibility defined in Eq. (9) that can be calculated theoretically [see Eq. (A13) in the Appendix], which also displays a peak as a function of t , as shown in Fig. 16(a) in the Appendix. Since in general t_s increases with the threshold W_{th} [see Fig. 4(b)], thus the irreversibility also peaks at some W_{th} as revealed in Figs. 9(a)–9(c) for $\langle \delta \rangle_{t_s}$. Using the KL-divergence measure for irreversibility, $\Delta_{KL}(t_s)$ defined in Eq. (9), with the stopping times t_s sampled from Langevin simulation trajectories, the average $\langle \Delta_{KL} \rangle_{t_s}$ is obtained as a function of W_{th} as shown in Fig. 8(c), also display maximal irreversibility at some W_{th} .

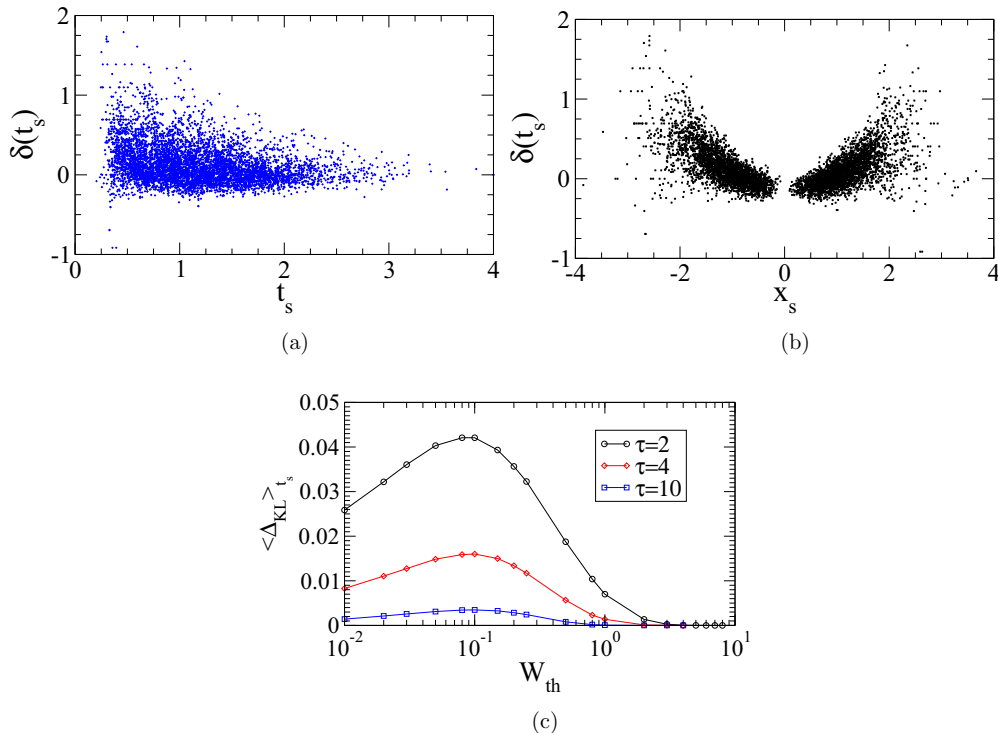


FIG. 8. Simulation results for the harmonic potential $U(x, \lambda(t)) = \frac{1}{2}\lambda(t)x^2$ with compressing protocol $\frac{\lambda(t)}{\lambda(0)} = 2 - \cos \frac{\pi t}{\tau}$. (a) $\delta(t_s)$ vs t_s and (b) $\delta(t_s)$ vs x_s for $W_{th} = 0.1$ and $\tau = 4$. (c) Δ_{KL} averaged over t_s sampled from the trajectories of the Langevin simulations plotted as a function of W_{th} for several values of τ .

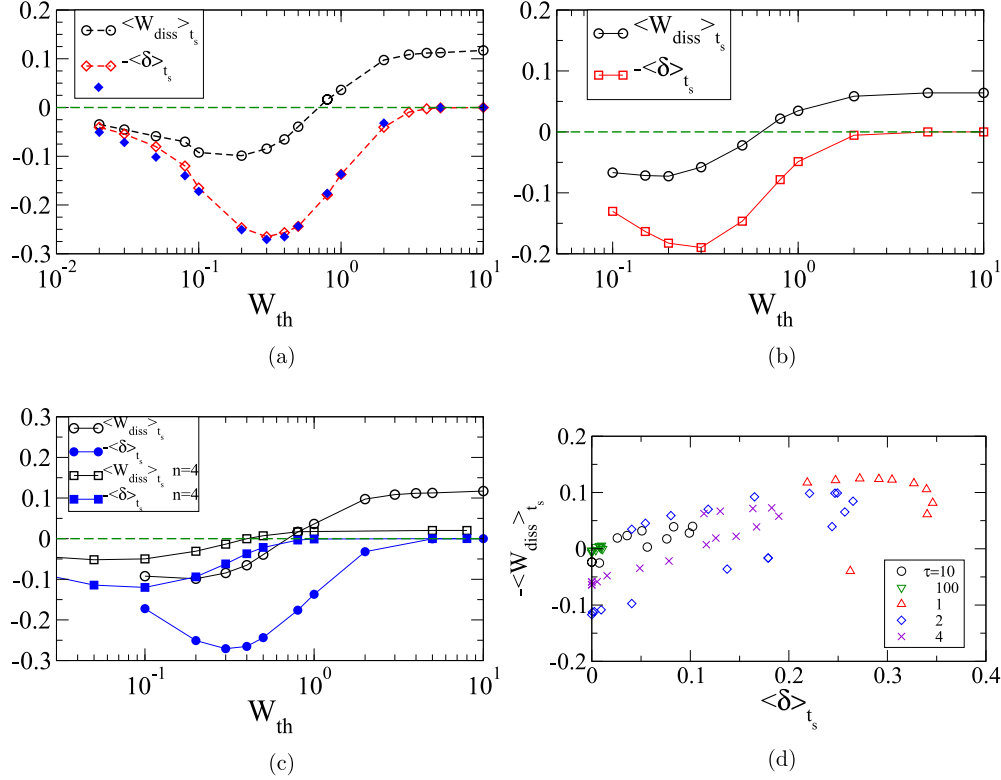


FIG. 9. Simulation results for the harmonic potential $U(x, \lambda(t)) = \frac{1}{2}\lambda(t)x^2$ with compressing protocol $\frac{\lambda(t)}{\lambda(0)} = 2 - \cos \frac{\pi t}{\tau}$. The uncertainties are estimated from several independent runs (typically five) and are about the size of the symbols. (a) $\langle W_{\text{diss}} \rangle_{t_s}$ and $-\langle \delta \rangle_{t_s}$ vs W_{th} . $\tau = 2$. The filled symbols (\blacklozenge) are results obtained using the theoretical result of $\delta(t)$ in Eq. (A12) and averaged over the stopping times in the simulation. (b) is similar to (a) but for $\tau = 4$. (c) $\langle W_{\text{diss}} \rangle_{t_s}$ vs W_{th} for the nonharmonic potential $U(x, \lambda(t)) = \frac{1}{2}\lambda(t)x^4$ with the same $\lambda(t)$ and $\tau = 2$. The case of harmonic potential is also shown for comparison. (d) $-\langle W_{\text{diss}} \rangle_{t_s}$ vs $\langle \delta \rangle_{t_s}$ for various values of τ .

The variation of irreversibility due to the action of the gambling demon as a function of the stopping threshold can be examined by plotting the simulation results of $-\langle \delta \rangle_{t_s}$ as a function of W_{th} in Figs. 9(a)–9(c). One can also compute $\langle \delta \rangle_{t_s}$ using the theoretical result of $\delta(t)$ in (A12) and averaged over the stopping times in the simulation, and the results are displayed in Fig. 9(a) (filled diamonds) showing good agreement. The averaged dissipative work is also displayed, showing that $\langle W_{\text{diss}} \rangle_{t_s} > -\langle \delta \rangle_{t_s}$ revealing that there is room to extract useful work (i.e., $\langle W_{\text{diss}} \rangle_{t_s} < 0$, winning) due to the highly irreversible nature of the process associated with the action of the demon. It is clear that $\langle \delta \rangle_{t_s}$ is always non-negative, exemplifying the second law of thermodynamics. For large values of W_{th} , $\langle \delta \rangle_{t_s}$ approaches zero since all trajectories can complete their journey and by definition $P(x, \tau) = P_R(x, 0)$. $\langle \delta \rangle_{t_s}$ is maximal at a threshold that is also close to a large negative mean dissipative work. This again reflects the situation that the demon is effective in winning in a highly irreversible scenario. Figure 9(d) plots $-\langle W_{\text{diss}} \rangle_{t_s}$ vs $\langle \delta \rangle_{t_s}$ for various values of τ , showing the general trend of more winning profit for stronger irreversibility.

A. Experimental test

To confirm the above theoretical and simulation results, we conducted experiments on the gambling demon under a squeezing harmonic potential. The experimental setup con-

sists of a 1- μm sized Brownian particle trapped in the squeezing potential controlled by the optical feedback trap [25]. The particle is first located in the equilibrium state for 50 ms, and the stiffness of the harmonic potential starts to increase from $\lambda=5$ pN/ μm to 15 pN/ μm for the process time τ according to the given protocol, Eq. (2), with $b = 1$. The relaxation time for this system is $\tau_R = \gamma/\lambda(0) \simeq 1.9\text{ms}$. At the end of the driving time τ , the stiffness of the potential starts to decrease according to the reverse protocol $\lambda_R(t)$. Figures 10(a)–10(c) are the time evolution of the particle position distributions in the squeezing potential and its reverse protocol for various process times. The initial equilibrium distribution gets sharper around the well center as the stiffness of the harmonic trap increases until the end of the forward process at $t = \tau$. Then, the stiffness immediately increases according to the reverse protocol for the same duration τ , and the distribution gets broadened. It is clear that the evolution of the distribution during the reverse process differs significantly from the forward one for small values of $\tau = 2$ ms and 4 ms, but such difference becomes rather small when the driving protocol is slow ($\tau = 10$ ms). The experimental stopped times are plotted against the stopped locations and are shown in Fig. 11(a) for various stopping thresholds, which is in agreement with the simulation results as shown in Fig. 3(c). The experimentally measured stopped position distributions for various stopping thresholds are shown in Fig. 11(b). For large W_{th} , $P(x_s)$ peaks at the well center

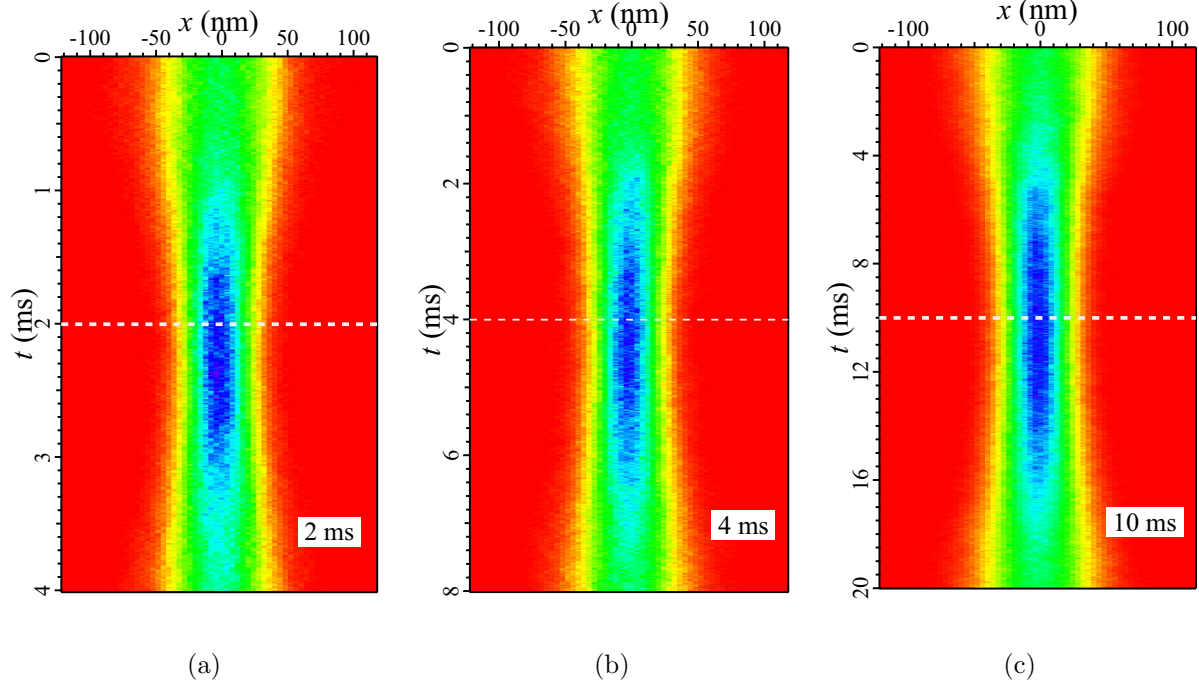


FIG. 10. Compressing harmonic protocol for the potential $U(x, \lambda(t)) = \frac{1}{2}\lambda(t)x^2$ with $\frac{\lambda(t)}{\lambda(0)} = 2 - \cos \frac{\pi t}{\tau}$. Experimental results on the evolution of position distributions during the process for $\tau =$ (a) 2 ms, (b) 4 ms, and (c) 10 ms. The horizontal dashed lines indicate the end of the forward process.

since almost all trajectories can complete their journeys. The peak of $P(x_s)$ becomes broadened as W_{th} decreases, and for small W_{th} , $P(x_s)$ is bimodal with most particles being stopped significantly away from the well center and only very few particles are stopped near the center. The experimental measured $P(x_s)$ agrees well with the simulation results shown in Fig. 3(d).

To examine the irreversibility of the squeezing harmonic trap experimentally, we measure the time evolution of the position variances of the forward and reverse protocols for various values of τ , as shown in Fig. 11(c). The difference between $w(0)$ and $w_R(\tau)$ increases for faster processes since the system is highly nonequilibrium and hence highly irreversible for small τ . The variances of the forward processes agree well with the analytical results from Eq. (A9) in the Appendix. The agreement of $w_R(t)$ with the theoretical result of Eq. (A11) in the Appendix for the reverse process is less satisfactory, especially for a small value of τ . Presumably, this is due to the fact that the initial state of the reverse protocol might deviate from the final state of the forward process (which is far from equilibrium) due to the finite response or delay times in the electronics of the experimental control. The average dissipative work $\langle W_{\text{diss}} \rangle_{t_s}$, which is related to the mean profit of the gambling demon, is measured experimentally as a function of the threshold for different values of τ 's, together with the average irreversibility $\langle \delta \rangle_{t_s}$, as shown in Figs. 12(a) and 12(b), which is in good agreement with the simulation results shown in Figs. 9(a) and 9(b). For fast processes (small τ), $\langle W_{\text{diss}} \rangle_{t_s}$ can achieve a more negative value in a regime of small W_{th} , indicating that more useful work (winning profit) can be extracted by the action of the demon. In addition, maximal winning can be achieved near the regime of higher

irreversibility $\langle \delta \rangle_{t_s}$. A plot of the experimental $\langle W_{\text{th}} \rangle_{t_s}$ vs $\langle \delta \rangle_{t_s}$ is shown in Fig. 12(c), which is in agreement with the simulation results (Fig. 9(d)) of the general trend of more winning profit for highly irreversible processes.

B. Stopping-time integral fluctuation theorem with internal degrees of freedom

The quantity δ in the gambling demon has been shown [20] to obey the stopping-time integral fluctuation relation

$$\langle e^{-W_{\text{diss}} - \delta} \rangle_{t_s} = 1, \quad (10)$$

which was verified experimentally for the single electron box system. From the Jensen inequality, Eq. (10) implies $\langle W_{\text{diss}} \rangle_{t_s} \geq -\langle \delta \rangle_{t_s}$ which explains why the demon has room to achieve winning. We shall examine the validity of the above fluctuation relation for the present gambling demon case of a Brownian particle in a squeezing trap. Figure 13 shows the simulation results of $\langle e^{-W_{\text{diss}}} \rangle_{t_s}$ and $\langle e^{-W_{\text{diss}} - \delta} \rangle_{t_s}$ as a function of the threshold for different values of τ . We also perform similar measurements experimentally, and the results are shown in Fig. 14(a). The experimental and simulation results indicate that $\langle e^{-W_{\text{diss}}} \rangle_{t_s}$ appreciably exceeds unity for smaller values of W_{th} implying the violation of the usual integral fluctuation theorem due to the stopping action of the demon, and a positive δ should be introduced to restore the integral fluctuation relation as suggested in Eq. (10). Furthermore, both the simulation and experimentally measured values of $\langle e^{-W_{\text{diss}} - \delta} \rangle_{t_s}$ are close to unity in most regimes, but for some regime of W_{th} , $\langle e^{-W_{\text{diss}} - \delta} \rangle_{t_s}$ is significantly less than unity. Such a deviation from Eq. (10) persists for different

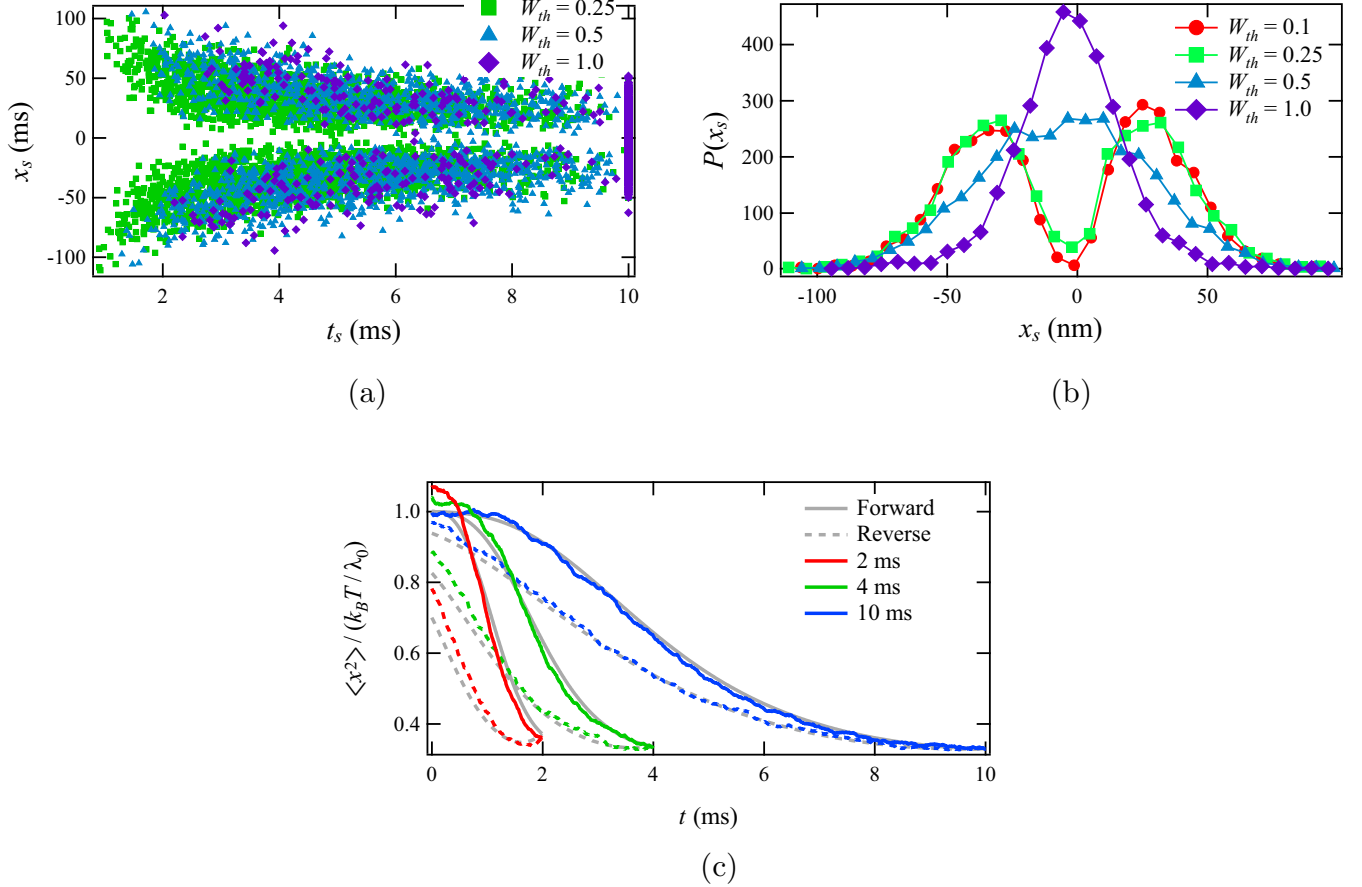


FIG. 11. (a) Experimental results of the stopped time t_s vs the stopped location x_s for various work thresholds W_{th} under the action of the gambling demon with $\tau=10$ ms. (b) The corresponding stopped location distributions $P(x_s)$ for the case in (a). (c) The variance evolution of particle positions of the forward (solid curves) and reverse (dashed curves) processes with $\tau = 2$ ms (red), 4 ms (green), and 10 ms (blue). The corresponding theoretical results are denoted by the grey curves.

values of τ 's and also for non-harmonic trapping potential [see Fig. 13(d)]. As discussed in the following, such discrepancy from the stopping-time integral fluctuation relation (10) can be attributed to the entropy production due to some internal degrees of freedom that were not taken into account.

To examine further theoretically, we consider the system setting consisting of the observed slow degrees of freedom (d.o.f.), which is the particle position $x(t)$ together with the internal and hidden d.o.f. (can be thought of as the fast Brownian kicks or other fast fluctuations in the experiments). Now the entropy production of the system includes the observed and internal contributions, written as $\Delta S_{\text{sys}} = \Delta S + \Delta S_{\text{int}}$, where quantities for the system, internal, and observed d.o.f. are denoted with the subscripts “sys”, “int” and no subscript, respectively. Here the energetics are in units of $k_B T$ and entropy is in units of k_B for convenience. The observed energetics are related by $\Delta U = W + Q$ and $\Delta F = \Delta U - \Delta S$. Hence, the observed dissipative work $W_{\text{diss}} = W - \Delta F = \Delta S + \Delta S_{\text{int}} - Q - \Delta S_{\text{int}} \equiv \Delta S_{\text{total}} - \Delta S_{\text{int}}$, where $\Delta S_{\text{total}} = \Delta S_{\text{sys}} - Q$ is the total entropy production of the environment plus the observed and internal d.o.f. Denote the coordinate of the internal d.o.f. by x_{int} , and the distribution functions of the system in the forward and reverse processes, respectively, by $\mathbf{P}(x, x_{\text{int}}, t)$ and $\mathbf{P}_R(x, x_{\text{int}}, t)$, the irreversibility of the system now is

related to $\delta(t)$ of the observed d.o.f. by

$$\delta_{\text{sys}}(t) = \ln \frac{\mathbf{P}(x(t), x_{\text{int}}(t), t)}{\mathbf{P}_R(x(t), x_{\text{int}}(t), \tau - t)} \quad (11)$$

$$= \ln \frac{P(x(t), t)}{P_R(x(t), \tau - t)} + \ln \frac{\mathcal{P}(x_{\text{int}}(t), t|x(t))}{\mathcal{P}_R(x_{\text{int}}(t), \tau - t|x(t))} \quad (12)$$

$$\equiv \delta(t) + \delta_{\text{int}}(t), \quad (13)$$

where \mathcal{P} and \mathcal{P}_R are the corresponding conditional probabilities. Then, invoking the Doob's optional stopping theorem [26], which states that for any Martingale stochastic variable $\mathcal{M}(t)$, $\langle \mathcal{M} \rangle_{t_s} = \langle \mathcal{M}(0) \rangle$. And since it has been shown in Ref. [20] that $e^{-\Delta S_{\text{total}} - \delta_{\text{sys}}}$ is Martingale, it follows that $e^{-W_{\text{diss}} - \delta_{\text{sys}} - \Delta S_{\text{int}}}$ is also Martingale. Hence together with Eq. (7) at $t = 0$, we have (since $W_{\text{diss}}(0) = \Delta S_{\text{int}} = 0$)

$$\langle e^{-W_{\text{diss}} - \delta_{\text{sys}} - \Delta S_{\text{int}}} \rangle_{t_s} = \langle e^{-\delta_{\text{sys}}(0)} \rangle = 1. \quad (14)$$

Hence if we define the effective internal entropy production $\Delta \tilde{S}_{\text{int}} \equiv \Delta S_{\text{int}} + \delta_{\text{int}}$, then Eq. (14) can be written as

$$\langle e^{-W_{\text{diss}} - \delta - \Delta \tilde{S}_{\text{int}}} \rangle_{t_s} = 1, \quad (15)$$

which is the generalized stopping time integral fluctuation theorem in terms of the observed W_{diss} and δ when the internal

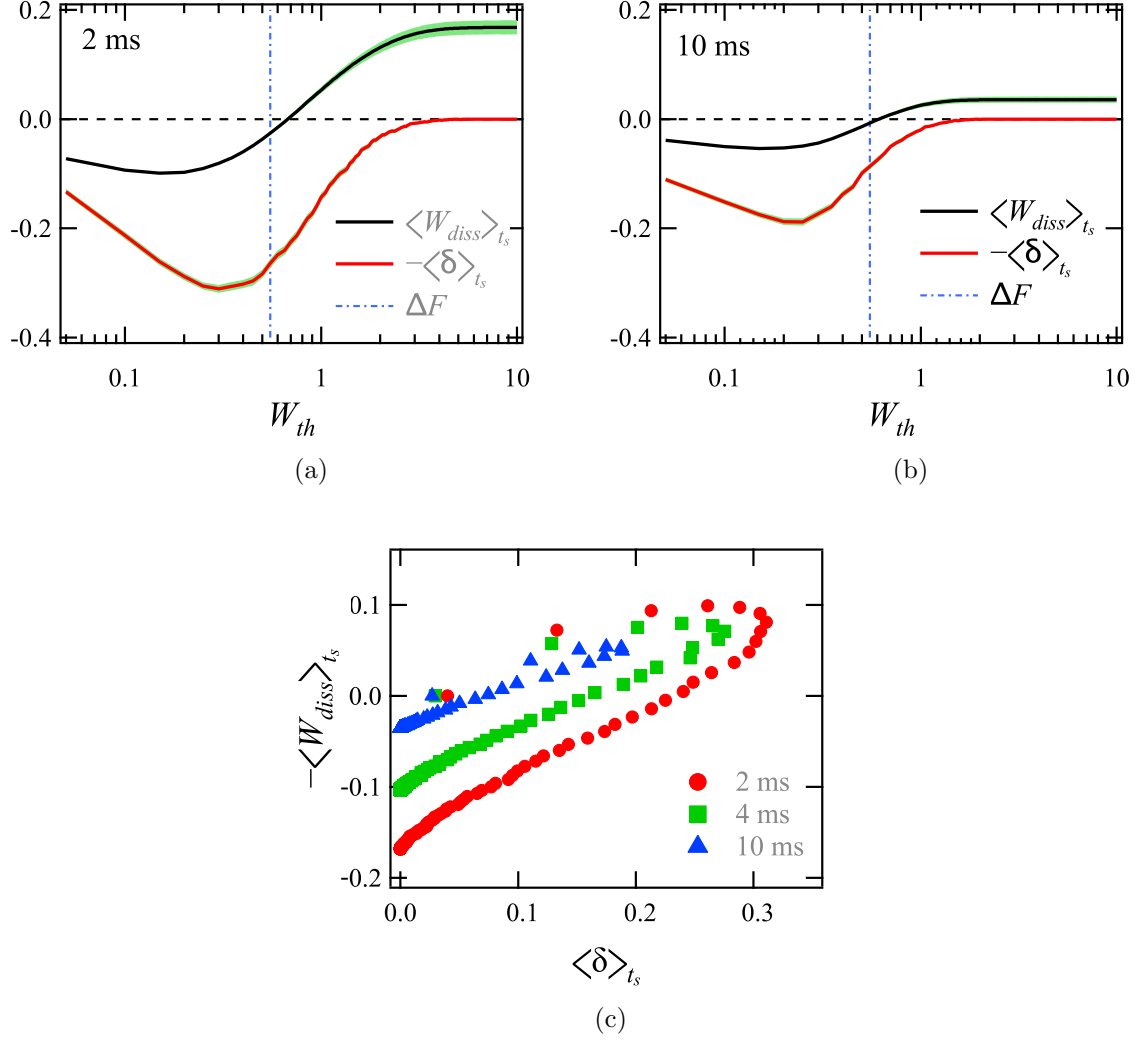


FIG. 12. Experimental results for $\langle W_{diss} \rangle_{t_s}$ (black line) and $\langle \delta \rangle_{t_s}$ (red line) as a function of W_{th} for $\tau =$ (a) 2 ms, (b) 10 ms. Error bars (green shadows) were obtained from bootstrap using 1000 resamplings of size 3000. (c) $-\langle W_{diss} \rangle_{t_s}$ as a function of $\langle \delta \rangle_{t_s}$ for $\tau = 2$ ms, 4 ms, and 10 ms.

d.o.f. is taken into account. In fact Eq. (15) has the same form as the stopping time integral fluctuation relation developed in Ref. [18] in the presence of some internal degrees of freedom. Now the experimental and simulation results [see Figs. 13 and 14(a)] can be understood in terms of Eq. (15) as follows. $\langle e^{-W_{diss}} \rangle_{t_s}$ significantly exceeds unity in regimes of smaller W_{th} in which many trajectories are stopped before completion. The stopping-time fluctuation theorem (15) can be rewritten as $\langle e^{-W_{diss}} e^{-(\delta + \Delta \tilde{S}_{int})} \rangle_{t_s}$. For the far-from-equilibrium situation considered here, one expects $\Delta \tilde{S}_{int}$ is negligible when compared with δ , hence $\delta + \Delta \tilde{S}_{int} \approx \delta > 0$ and thus $\langle e^{-W_{diss}} \rangle_{t_s} > 1$. For large W_{th} in which most trajectories can complete, both $\delta \approx 0$ (since $\delta(\tau) = 0$) and $\Delta \tilde{S}_{int} \approx 0$ (since $t_s \simeq \tau$ and all internal d.o.f. are well equilibrated), then $\langle e^{-W_{diss}} \rangle_{t_s} \rightarrow \langle e^{-\Delta S_{total}} \rangle = 1$, which follows from the usual integral fluctuation theorem. On the other hand, the experimental and simulation results of $\langle e^{-W_{diss} - \delta} \rangle_{t_s} < 1$ in some intermediate values of W_{th} [see Figs. 13 and 14(a)] suggest that in this regime, there is a non-negligible negative effective entropy production of the internal d.o.f., i.e., $\Delta \tilde{S}_{int} < 0$, which can be

understood intuitively with the following physical picture: For intermediate values of W_{th} , a large portion of the trajectories are stopped with very short t_s [see Fig. 3(e)] for the distribution of the stopping times) and the internal d.o.f. cannot be fully relaxed. In addition, such early-stopped trajectories receive not many strong thermal kicks with the work already reaching W_{th} in a very short time. These early-stopped trajectories sampled by our gambling demon are biased with strong directional ballistic kicks that push the particle far from the trapping center. In other words, the fast d.o.f. in the environment near the particle are in a much orderly fashion as compared to the initial $t = 0$ situation, thus there would be a decrease in the corresponding entropy leading to $\Delta \tilde{S}_{int} < 0$. To verify the above scenario, we measure experimentally the position distribution of the trajectories before some stopped times within a time window of 2 ms as shown in Fig. 14(b). For large stopping times, the particle trajectory is located predominantly around the well center. But the particle trajectory stays far away from the well center if the particle is stopped at an early time, as described in the above picture.

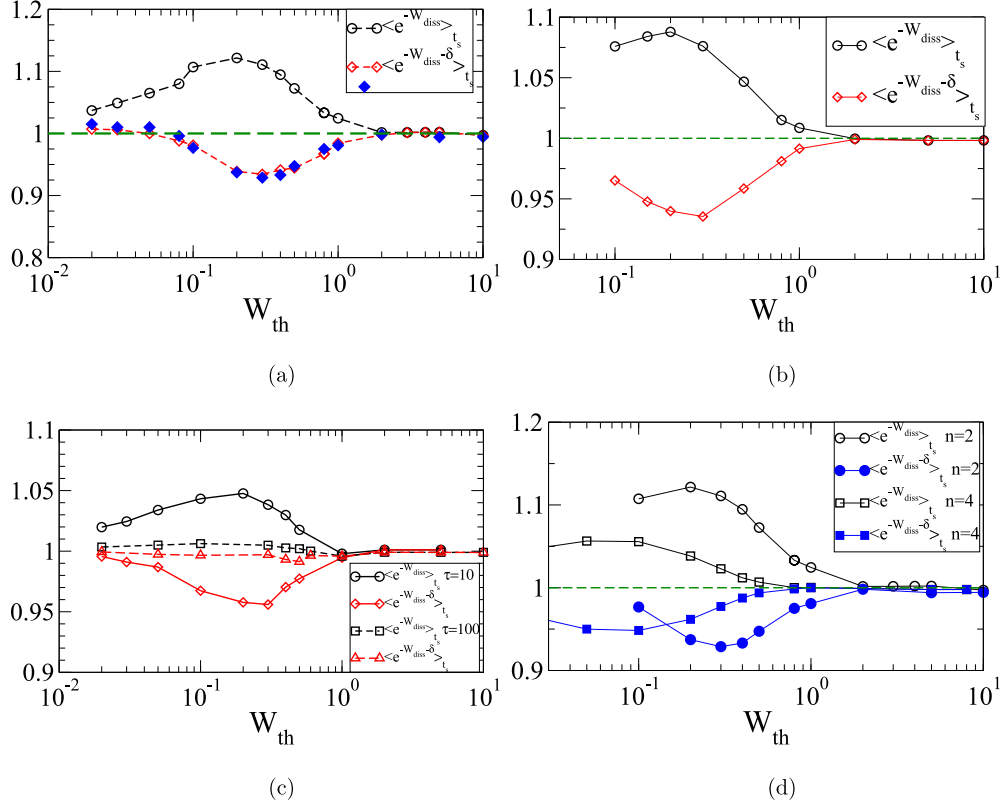


FIG. 13. Compressing harmonic protocol for the potential $U(x, \lambda(t)) = \frac{1}{2}\lambda(t)x^2$ with $\frac{\lambda(t)}{\lambda(0)} = 2 - \cos \frac{\pi t}{\tau}$. (a) $\langle e^{-W_{diss}} \rangle_{t_s}$ and $\langle e^{-W_{diss}-\delta} \rangle_{t_s}$ vs W_{th} for $\tau = 2$. The filled symbols (\blacklozenge) are results obtained using the theoretical result of $\delta(t)$ in Eq. (A12) and averaged over the stopping times in the simulation. (b) $\langle e^{-W_{diss}} \rangle_{t_s}$ and $\langle e^{-W_{diss}-\delta} \rangle_{t_s}$ vs W_{th} for $\tau = 4$. (c) is similar to (a) and (b) but for $\tau = 10$ and 100 . (d) $\langle e^{-W_{diss}} \rangle_{t_s}$ and $\langle e^{-W_{diss}-\delta} \rangle_{t_s}$ vs W_{th} for the nonharmonic potential $U(x, \lambda(t)) = \frac{1}{2}\lambda(t)x^4$ with the same $\lambda(t)$ and $\tau = 2$. The case of a harmonic potential is also shown for comparison. The uncertainties are estimated from several independent runs (typically five) and are about the size of the symbols.

Finally, from the measured $\langle e^{-W_{diss}-\delta} \rangle_{t_s}$ and stopping time integral fluctuation theorem (15), one can give an order of magnitude estimate of the maximal value of $\Delta\tilde{S}_{int}$ (in unit of k_B): $1 = \langle e^{-W_{diss}-\delta-\Delta\tilde{S}_{int}} \rangle_{t_s} \approx \langle e^{-W_{diss}-\delta} \rangle_{t_s} e^{-\Delta\tilde{S}_{int}}$, and with $\langle e^{-W_{diss}-\delta} \rangle_{t_s} \simeq 0.92$ to 0.95 , one then gets $\Delta\tilde{S}_{int} \sim -0.08$ to -0.05 .

V. CONCLUSION

In this paper, the energetics including the average dissipative work, the distributions of the stopping positions, and stopping times of a Brown particle in a squeezing potential under the action of a gambling demon with a prescribed work threshold are investigated by simulations and also measured

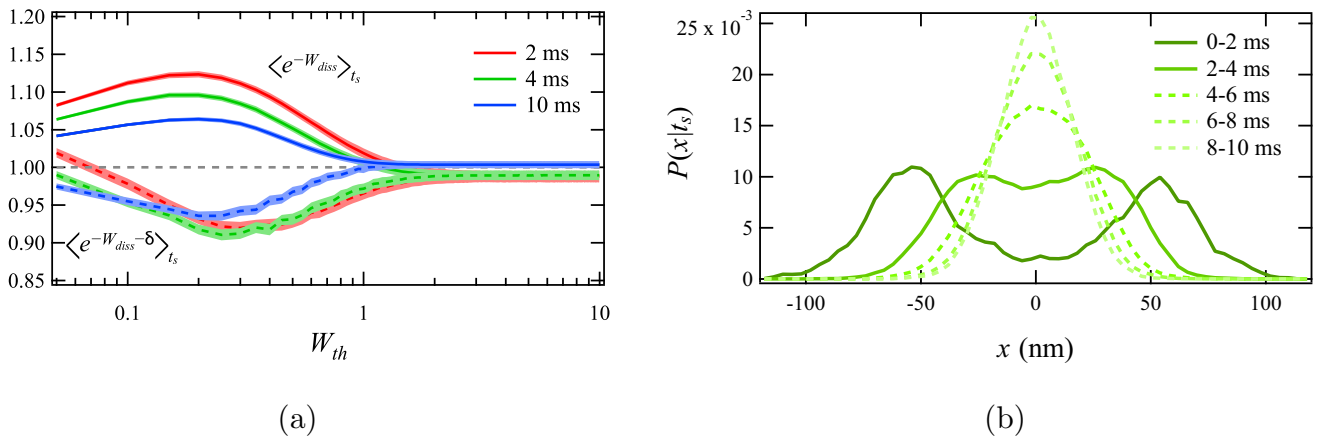


FIG. 14. Experimental results of the compressing harmonic potential for $\tau=2$ ms, 4 ms and 10 ms. (a) $\langle e^{-W_{diss}} \rangle_{t_s}$ (solid curves) and $\langle e^{-W_{diss}-\delta} \rangle_{t_s}$ (dashed curves) vs W_{th} . Error bars (shadows) were obtained from bootstrap using 1000 resamplings of size 3000. (b) The position distribution of trajectories before different stopped times within a time window of 2ms. $\tau = 10$ ms and $W_{th} = 0.25$.

experimentally. A strongly irreversible process is essential for the demon to be effective in winning. The degree of irreversibility of the process is further studied by investigating the time-reversed protocol of expanding the potential trap. The time-dependent variance of the position distributions of the forward and reverse processes together with the quantity δ are employed to quantify the irreversibility. The stopping-time fluctuation relation, which involves W_{diss} and δ , is also examined for a broad range of stopping threshold W_{th} . Both the simulation result and experimental measurements found that the stopping-time fluctuation relation can be reconciled with a significant negative internal entropy production associated with hidden internal degrees of freedom in some regime of W_{th} .

ACKNOWLEDGMENTS

This work has been supported by the National Science and Technology Council of Taiwan under Grants No. 112-2112-M-008-030- (Y.J.) and No. 110-2112-M008-026-MY3 (P.-Y.L.).

APPENDIX: MEAN ENERGETICS, TIME-DEPENDENT POSITION DISTRIBUTIONS AND MEAN IRREVERSIBILITY FOR $U(x, \lambda(t)) = \frac{1}{2}\lambda(t)x^2$

Under the protocol of ramping the stiffness of the harmonic trap, the particle distribution function does not follow the Boltzmann distribution due to the time-dependent variation that leads to nonequilibrium behavior. But the distribution is still Gaussian [27,28] with

$$P(x, t) = \sqrt{\frac{\beta}{2\pi w(t)}} e^{-\frac{\beta x^2}{2w(t)}}, \quad (\text{A1})$$

where $\beta = 1/(k_B T)$ and $w(t)$ satisfies

$$\dot{w} = \frac{2}{\gamma}(1 - \lambda(t)w(t)). \quad (\text{A2})$$

For arbitrary $\lambda(t)$, w can be solved to give

$$w(t) = e^{-\frac{2}{\gamma} \int_0^t ds \lambda(s)} \left[w(0) + \frac{2}{\gamma} \int_0^t du e^{\frac{2}{\gamma} \int_0^u ds \lambda(s)} \right]. \quad (\text{A3})$$

The mean change in internal energy is given by

$$\beta \langle \Delta U(t) \rangle = \frac{1}{2}(\lambda(t)w(t) - \lambda(0)w(0)) = \frac{1}{2}(\lambda(t)w(t) - 1), \quad (\text{A4})$$

where the last equality holds if the initial state is at equilibrium. The mean cumulative work at time t can be calculated as

$$\beta \langle W(t) \rangle = \frac{1}{2} \int_0^t \dot{\lambda}(s) w(s) ds. \quad (\text{A5})$$

Integrating by parts upon Eq. (A5) and invoking Eq. (A4) and the First Law of thermodynamics, one obtains the mean heat flow into the system

$$\beta \langle Q(t) \rangle = \frac{1}{2} \int_0^t \lambda(s) \dot{w}(s) ds = \frac{1}{\gamma} \int_0^t \lambda(s) [1 - \lambda(s)w(s)] ds, \quad (\text{A6})$$

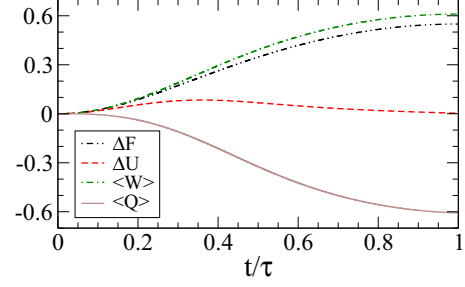


FIG. 15. Time dependence of the mean energetics for the compressing harmonic protocol for the potential $U(x, \lambda(t)) = \frac{1}{2}\lambda(t)x^2$ with $\frac{\lambda(t)}{\lambda(0)} = 2 - \cos \frac{\pi t}{\tau}$ with $\tau = 4$.

where the last equality follows from Eq. (A2). For $\lambda(t) = \lambda(0)[1 + b(1 - \cos \frac{\pi t}{\tau})]$, one has

$$\begin{aligned} \int_0^t \lambda(s) ds &= \lambda(0) \left[(1+b)t - \frac{b\tau}{\pi} \sin \frac{\pi t}{\tau} \right], \\ \int_0^t \lambda(\tau - s) ds &= \lambda(0) \left[(1+b)t + \frac{b\tau}{\pi} \sin \frac{\pi t}{\tau} \right]. \end{aligned} \quad (\text{A7})$$

Together with $\beta \Delta F(t) = \frac{1}{2} \ln \frac{\lambda(t)}{\lambda(0)} = \frac{1}{2} \ln [1 + b(1 - \cos \frac{\pi t}{\tau})]$, all the time-dependent mean energetics can then be theoretically calculated. It will be convenient to express all times in units of $\tau_R \equiv \gamma/\lambda(0)$, lengths in units of $\sqrt{k_B T/\lambda(0)}$ and energies in units of $k_B T$ for numerical results. Figure 15 shows the theoretical results of the mean time-dependent energetics as a function of time during the squeezing of the harmonic potential.

For the case of harmonic trapping potential, the time-dependent position distribution is still Gaussian [27,28] with

$$P(x, t) = \sqrt{\frac{\beta}{2\pi w(t)}} e^{-\frac{\beta x^2}{2w(t)}}, \quad (\text{A8})$$

where $\beta = 1/(k_B T)$ and $w(t)$ satisfies $\dot{w} = \frac{2}{\gamma}(1 - \lambda(t)w(t))$. For arbitrary $\lambda(t)$, w can be solved to give

$$w(t) = e^{-\frac{2}{\gamma} \int_0^t ds \lambda(s)} \left[w(0) + \frac{2}{\gamma} \int_0^t du e^{\frac{2}{\gamma} \int_0^u ds \lambda(s)} \right]. \quad (\text{A9})$$

For the reverse process with $\lambda_R(t) = \lambda(\tau - t)$, the distribution function is similarly given by

$$P_R(x, t) = \sqrt{\frac{\beta}{2\pi w_R(t)}} e^{-\frac{\beta x^2}{2w_R(t)}} \quad (\text{A10})$$

with $w_R(t)$ satisfies $\dot{w}_R = \frac{2}{\gamma}(1 - \lambda(\tau - t)w_R(t))$ with the initial condition $w_R(0) = w(\tau)$. w_R can be solved similarly to give

$$\begin{aligned} w_R(\tau - t) &= e^{-\frac{2}{\gamma} \int_0^{\tau-t} ds \lambda(\tau-s)} \left[w(\tau) + \frac{2}{\gamma} \int_0^{\tau-t} du e^{\frac{2}{\gamma} \int_0^u ds \lambda(\tau-s)} \right]. \end{aligned} \quad (\text{A11})$$

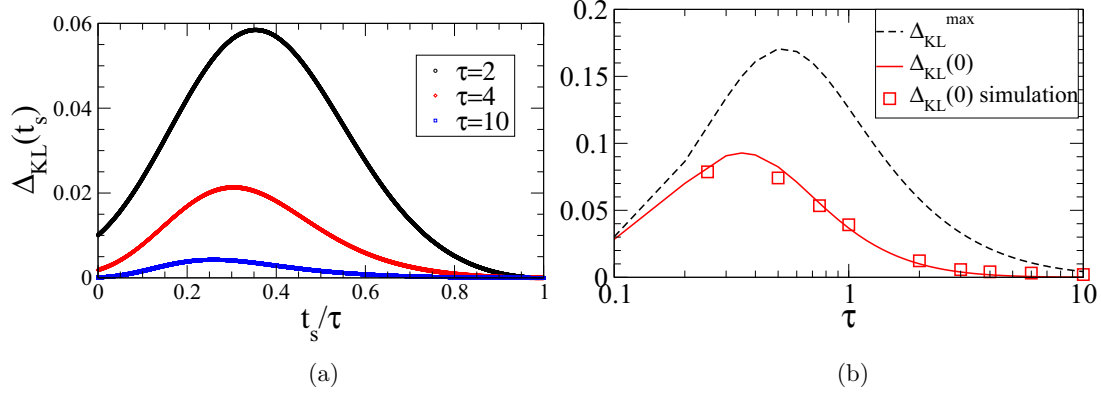


FIG. 16. Harmonic potential $U(x, \lambda(t)) = \frac{1}{2}\lambda(t)x^2$ with compressing protocol $\frac{\lambda(t)}{\lambda(0)} = 2 - \cos \frac{\pi t}{\tau}$. (a) Theoretical result of $\Delta_{KL}(t)$ calculated from Eqs. (A9), (A11), and (A13) for several values of τ . (b) Theoretical results for the peak value of Δ_{KL} and $\Delta_{KL}(0)$ vs τ . The simulation results of $\Delta_{KL}(0)$ (symbol) are also shown.

Finally, from Eq. (6), the irreversibility for a trajectory at a time t is then given by

$$\delta(t) = \frac{\beta x^2(t)}{2} \left[\frac{1}{w_R(\tau - t)} - \frac{1}{w(t)} \right] + \frac{1}{2} \ln \left(\frac{w_R(\tau - t)}{w(t)} \right). \quad (\text{A12})$$

And the average irreversibility at time t

$$\langle \delta(t) \rangle \equiv \Delta_{KL}(t) = \frac{1}{2} \left[\frac{w(t)}{w_R(\tau - t)} - 1 \right] + \frac{1}{2} \ln \left(\frac{w_R(\tau - t)}{w(t)} \right), \quad (\text{A13})$$

which can be theoretically computed directly using Eqs. (A9) and (A11) and is plotted in Fig. 16(a) showing a peak in $\Delta_{KL}(t)$ for some optimal value of t_m which can be calculated analytically by setting $\Delta'_{KL}(t_m) = 0$ in Eq. (A13) and invoking Eqs. (A9) and (A11) to give

$$\frac{1}{w(t_m)} + \frac{1}{w_R(\tau - t_m)} = 2\lambda(t_m). \quad (\text{A14})$$

The optimal value of t_m and the corresponding value of maximal irreversibility $\Delta_{KL}(t_m)$, can then be obtained theoretically and is shown in Fig. 16(b) as a function of τ . It is worth noting that $\Delta_{KL}(t_m)$ itself also peaks at $\tau \simeq 0.5$, suggesting for protocol with τ around this value, the system is maximally irreversible and the gambling demon would have a good chance to win. It is also easy to verify the second Law from Eq. (A13) since $\langle \delta(t) \rangle = \Delta_{KL}(t) = \frac{1}{2} \left(\frac{w(t)}{w_R(\tau - t)} - 1 - \ln \frac{w(t)}{w_R(\tau - t)} \right) \geq 0$. One can also explicitly verify the integral fluctuation relation (7) by directly calculating using Eqs. (A12) and noting that the distribution $P(x, t)$ is given by Eq. (A1)

$$\langle e^{-\delta(t)} \rangle = \sqrt{\frac{w(t)}{w_R(\tau - t)}} \left\langle e^{-\frac{\beta}{2} \left(\frac{1}{w_R(\tau - t)} - \frac{1}{w(t)} \right) x^2(t)} \right\rangle \quad (\text{A15})$$

$$= \sqrt{\frac{\beta}{2\pi w_R(\tau - t)}} \int dx e^{-\frac{\beta}{2} x^2 \frac{1}{w_R(\tau - t)}} = 1. \quad (\text{A16})$$

-
- [1] G. Gallavotti and E. G. D. Cohen, Dynamical ensembles in nonequilibrium statistical mechanics, *Phys. Rev. Lett.* **74**, 2694 (1995).
- [2] C. Jarzynski, Equilibrium free-energy differences from nonequilibrium measurements: A master-equation approach, *Phys. Rev. E* **56**, 5018 (1997).
- [3] G. E. Crooks, Entropy production fluctuation theorem and the nonequilibrium work relation for free energy differences, *Phys. Rev. E* **60**, 2721 (1999).
- [4] U. Seifert, Entropy production along a stochastic trajectory and an integral fluctuation theorem, *Phys. Rev. Lett.* **95**, 040602 (2005).
- [5] K. Sekimoto, *Stochastic Energetics*, Volume 799 of Lecture Notes in Physics (Springer, Berlin, 2010).
- [6] D. Collin, Jr., F. Ritort, C. Jarzynski, S. B. Smith, I. Tinoco, and C. Bustamante, Verification of the Crooks fluctuation theorem and recovery of RNA folding free energies, *Nature (London)* **437**, 231 (2005).
- [7] J. V. Koski, T. Sagawa, O.-P. Saira, Y. Yoon, A. Kutvonen, P. Solinas, M. Möttönen, T. Ala-Nissila, and J. P. Pekola, Distribution of entropy production in a single-electron box, *Nat. Phys.* **9**, 644 (2013).
- [8] Y. Jun, M. Gavrilov, and J. Bechhoefer, High-precision test of Landauer's principle in a feedback trap, *Phys. Rev. Lett.* **113**, 190601 (2014).
- [9] S. Ciliberto, Experiments in stochastic thermodynamics: Short history and perspectives, *Phys. Rev. X* **7**, 021051 (2017).
- [10] J. A. C. Albay, S. R. Wulaningrum, C. Kwon, P.-Y. Lai, and Y. Jun, Thermodynamic cost of a shortcuts-to-isothermal transport of a Brownian particle, *Phys. Rev. Res.* **1**, 033122 (2019).
- [11] Y. Jun and P.-Y. Lai, Instantaneous equilibrium transition for Brownian systems under time-dependent temperature and potential variations: Reversibility, heat and work relations, and fast isentropic process, *Phys. Rev. Res.* **3**, 033130 (2021).
- [12] H. Touchette, The large deviation approach to statistical mechanics, *Phys. Rep.* **478**, 1 (2009).
- [13] U. Seifert, Stochastic thermodynamics, fluctuation theorems and molecular machines, *Rep. Prog. Phys.* **75**, 126001 (2012).
- [14] L. Peliti and S. Pigolotti, *Stochastic Thermodynamics: An Introduction* (Princeton University Press, Princeton, NJ, 2021).

- [15] Y. Jun and P.-Y. Lai, Minimal dissipation protocols of an instantaneous equilibrium Brownian particle under time-dependent temperature and potential variations, *Phys. Rev. Res.* **4**, 023157 (2022).
- [16] S. P. I. Neri, É. Roldán, and F. Jülicher, Integral fluctuation relations for entropy production at stopping times, *J. Stat. Mech.* (2019) 104006.
- [17] G. Manzano and É. Roldán, Survival and extreme statistics of work, heat, and entropy production in steady-state heat engines, *Phys. Rev. E* **105**, 024112 (2022).
- [18] I. Neri, Second law of thermodynamics at stopping times, *Phys. Rev. Lett.* **124**, 040601 (2020).
- [19] I. Neri, Universal tradeoff relation between speed, uncertainty, and dissipation in nonequilibrium stationary states, *SciPost Phys.* **12**, 139 (2022).
- [20] G. Manzano, D. Subero, O. Maillet, R. Fazio, J. P. Pekola, and É. Roldán, Thermodynamics of gambling demons, *Phys. Rev. Lett.* **126**, 080603 (2021).
- [21] J. A. C. Albay, Y. Jun, and P.-Y. Lai, Winning strategies of a gambling demon in a Brownian particle under a squeezing potential, *Phys. Rev. Res.* **5**, 023115 (2023).
- [22] E. Roldan *et al.*, Martingales for physicists: A treatise on stochastic thermodynamics and beyond, [arXiv:2210.09983](https://arxiv.org/abs/2210.09983).
- [23] H. B. Callen, *Thermodynamics and An Introduction to Thermostatistics* (Wiley, New York, 1985).
- [24] R. Landauer, Irreversibility and heat generation in the computing process, *IBM J. Res. Dev.* **5**, 183 (1961).
- [25] J. A. C. Albay, G. Paneru, H. K. Pak, and Y. Jun, Optical tweezers as a mathematically driven spatio-temporal potential generator, *Opt. Express* **26**, 29906 (2018).
- [26] J. Doob, *Stochastic Processes* (Wiley, New York, 1953).
- [27] I. A. Martínez, A. Petrosyan, D. Guéry-Odelin, E. Trizac, and S. Ciliberto, Engineered swift equilibration of a Brownian particle, *Nat. Phys.* **12**, 843 (2016).
- [28] J. A. C. Albay, P.-Y. Lai, and Y. Jun, Realization of finite-rate isothermal compression and expansion using optical feedback trap, *Appl. Phys. Lett.* **116**, 103706 (2020).